THE APPLICATION OF PHYSICAL PRINCIPLES IN COOLING THERMAL MANAGEMENT OF ELECTRIC VEHICLE ELECTRONIC EQUIPMENT

by

Chen WANG *

Qinghai Minzu University, Xining, China

Original scientific paper
https://doi.org/10.2298/TSCI2506177W

This paper focuses on the application of physical principles in the cooling and thermal management of electric vehicle electronic equipment, examining the thermal management problems caused by the increasing power density of electronic equipment. First, the heat generation mechanism of power electronic devices and battery systems is analyzed, and the application of heat conduction, convection, and radiation principles in cooling is explained. Innovatively construct a multi-physics field coupling algorithm and an artificial intelligence-based thermal management strategy optimization algorithm, and compare and analyze the temperature distribution and cooling system performance under different working conditions through the construction of an experimental platform and the establishment of a simulation model. The simulation results demonstrate that the proposed algorithm can accurately simulate the heating and heat dissipation processes, with a temperature prediction error controlled within 3%. Experimental verification shows that the multi-physics coupling algorithm achieves <3% error by dynamically coupling heat transfer, fluid-flow, and electrical fields, outperforming traditional methods (error >5%) as confirmed by experimental-simulation comparisons experimental-simulation comparisons. The research provides theoretical and technical support for efficient thermal management of electric vehicle electronic equipment.

Key words*: electric vehicle, electronic equipment, thermal management, physical principle, multi-physics field coupling algorithm, experimental simulation, artificial intelligence*

Introduction

With the iteration of electric vehicle technology, the power density of power electronic devices and battery systems has increased, and thermal management has become a bottleneck for performance improvement. The power density of the current mainstream electric vehicle IGBT module exceeds 200 W/cm², the energy density of the power battery reaches more than 300 Wh/kg, and the heat generation per unit volume has doubled compared to five years ago. Overheating of the equipment will increase the switching loss of the power device by 15%-20%, and the battery cycle life will be reduced by more than 30%. When the battery pack exceeds 45°C in summer, the capacity decay accelerates by 50%, and the probability of thermal runaway increases to three times the normal level [1]. Efficient thermal management is crucial to a vehicle's endurance, safety, and overall experience.

Existing research primarily focuses on optimizing a single cooling method, while the analysis of the heat transfer mechanism under the interaction of multiple physical fields

* Author's e-mail: wangchen568@163.com

remains insufficient [2]. When traditional simulation algorithms couple various characteristics, the calculation accuracy is inadequate (the error exceeds 5%), and the iteration efficiency is low [3]. For example, when simulating ignore temperature-dependent resistance (IGBT) modules, the effect of temperature on resistance is ignored, resulting in large deviations. Traditional algorithms IGBT and fluid property changes, causing 5%-8% errors. Our coupled model addresses these factors, cutting error to <3%. In scenarios with multiple heat sources, existing strategies struggle to accurately distribute the load, resulting in an energy utilization rate of only 60%-70 % for the cooling system.

This study proposes a multi-physics field coupling simulation framework that collaboratively solves related equations, dynamically couples and simulates the heat transfer process, and improves calculation accuracy by more than 40% compared to the traditional method. The deep reinforcement learning algorithm is introduced to build an intelligent control model, which optimizes the system within 0.1 second and improves the system's energy efficiency by 25%. Experiments show that the micro-channel structure combined with topology optimization can reduce the temperature of the IGBT module by 10-15 °C and improve the heat dissipation uniformity by 35% under the same power consumption. The verification system established in the study verifies the reliability of the method and lays the foundation for the development of related technologies.

Heat generation mechanism of the electric vehicle's electronic equipment

Analysis of main heat source components

Power electronic devices

Define the non-linear relationship between switching loss and junction temperature and current, and obtain the switching loss calculation formula [4]:

$$P_{\mathrm{sw}} = k_{\mathrm{sw}} I^m V_{\mathrm{dc}}^n f \exp\left[-\alpha\left(T_j - T_{\mathrm{ref}}\right)\right] \tag{1}$$

where k_{sw} is the switching loss coefficient, I – the on-current, V_{dc} – the DC bus voltage, f – the switching frequency, T_j – the junction temperature, T_{ref} – the reference temperature, α – the temperature coefficient, and m and n – the non-linear exponents (value range 1.2-1.5) [5]. The $k_{\mathrm{sw}} = 0.8 \cdot 10^{-6}$, $\alpha = 0.002$ K^{-1}, $m = 1.3$, and $n = 1.2$ (calibrated via 100+ tests on 1200V IGBT modules), ensuring 95% agreement with manufacturer's loss data. The conduction loss is related to the temperature characteristics of the on-resistance, and its original calculation equation is:

$$P_{\mathrm{on}} = I^2 R_{\mathrm{on0}}\left[1 + \beta\left(T_j - T_{\mathrm{ref}}\right) + \gamma\left(T_j - T_{\mathrm{ref}}\right)^2\right] \tag{2}$$

where R_{on0} is the on-resistance at the reference temperature and β and γ are the linear and quadratic temperature coefficients, respectively.

Battery system

A heat generation model considering the coupling effect of SOC and temperature is constructed, and its total heat generation power formula is:

$$Q = I^2 R_{\mathrm{int}}\left(SOC, T\right) + IT\frac{\partial U_{\mathrm{ocp}}}{\partial T} \tag{3}$$

where R_{int}(SOC, T) is the internal resistance function that changes with SOC and temperature, U_{ocp} – the open circuit voltage, and $\partial U_{\mathrm{oc}}\mathrm{p}/\partial T$ – the entropy thermal coefficient [6]. Entropy term

contributes 5%-15% of total heat (25 °C, SOC 80%), validated via calorimeter tests, improving model accuracy by 8% *vs*. resistive-only models. The non-linear expression of the internal resistance function is obtained by fitting the experimental data:

$$R_{\text{int}}\left(SOC,T\right)=R_0\left[a+bSOC+cSOC^2\right]\exp\left[-d\left(T-25\right)\right] \tag{4}$$

where R_0 is the reference internal resistance, a, b, c – the SOC influence coefficients, and d – the temperature coefficient.

Physical principles of heat generation

Principle of resistive heating

Resistive heating of electronic equipment follows Joule's law, but the temperature dependence of material resistivity must be considered in practical applications. The resistivity of metal conductors increases with increasing temperature, resulting in a non-linear change in heating power. Define the resistance temperature characteristic function:

$$R\left(T\right)=R_0\left(1+\alpha_T T+\beta_T T^2\right)$$

and combine it with the instantaneous current, $i(t)$, to get the thermal power expression under variable temperature conditions:

$$P\left(t\right)=i(t)^2 R_0\left[1+\alpha_T T\left(t\right)+\beta_T T(t)^2\right] \tag{5}$$

where α_T = 0.0039 K^{-1} (linear temperature coefficient) and β_T = 1.2 10–5 K^{-2} (quadratic) for copper, derived from 20-150 °C resistance tests per ASTM B193 standards. The total heat generated in a specific period can be obtained by integrating the time:

$$Q=\int_{t_1}^{t_2} i(t)^2 R_0\left[1+\alpha_T T\left(t\right)+\beta_T T(t)^2\right]\mathrm{d}t \tag{6}$$

This formula breaks through the traditional assumption of constant resistance and is more in line with the actual working state of electronic devices.

Heating mechanism of semiconductor deviceshe

heat generated by semiconductor devices comes from the energy dissipation in the carrier transport process [7]. The heating model based on carrier concentration distribution can be expressed:

$$q=q_n+q_p=q_0\left[n\left(x\right)\mu_n+p\left(x\right)\mu_p\right]E(x)^2 \tag{7}$$

where q_n and q_p are the heat flux densities contributed by electrons and holes, respectively, $n(x)$, $p(x)$ – the carrier concentrations, μn, μp – the mobilities, and $E(x)$ – the electric field strength. Mobility decreases with increasing temperature [8].

Physical principles applicable to cooling of electronic equipment in electric vehicles

Principles and applications of heat conduction

Basic theory of heat conduction

Heat conduction is the primary method by which electronic equipment dissipates heat, and its essence lies in the energy transfer caused by molecular thermal motion. Fourier's law describes the linear relationship between heat flux and temperature gradient. However, in the

actual heat dissipation process, the thermal conductivity of the material changes with temperature and micro-structure [9]. Considering the thermal conductivity characteristics of multi-tropic materials, a 3-D heat conduction equation can be established:

$$q = -\nabla\left[k(T)\nabla T\right] \tag{8}$$

where $k(T)$ is the temperature-dependent thermal conductivity, for graphene-reinforced composite materials, its expression can be written as $k(T) = k_0(1 + a\ln T + bT0.5)$, where k_0 is the base thermal conductivity, and a and b are temperature coefficients. Logarithmic term captures phonon-scattering at high temperatures ($T > 300$ K), reducing $k(T)$ prediction error from 12% (linear model) to 4% (this model), validated via laser flash analysis.

Application in heat dissipation design

The liquid cold plate is a key component for heat dissipation of electronic equipment, and its internal flow channel structure directly affects the heat conduction efficiency. The total thermal resistance of the liquid cold plate is composed of material thermal resistance based on the thermal resistance network theory, contact thermal resistance and convection thermal resistance. Define the liquid cold plate thermal resistance calculation model:

$$R_{\text{total}} = \frac{\delta}{k_{\text{plate}}A} + R_{\text{contact}} + \frac{1}{hA} \tag{9}$$

where δ is the thickness of the liquid cooling plate, k_{plate} – the thermal conductivity of the plate, A – the heat transfer area, R_{contact} – the contact thermal resistance, and h – the convection heat transfer coefficient.

Principle and application of thermal convection

Basic concept of thermal convection

Thermal convection transfers heat through fluid-flow, and forced convection is the primary mechanism for cooling systems in electric vehicles [10]. Newton's Law of Cooling describes the relationship between convective heat transfer and the temperature difference. Considering the change of fluid properties with temperature, it can be corrected to:

$$Q = h(T)A\left(T_w - T_f\right) \tag{10}$$

where $h(T)$ is the temperature-dependent heat transfer coefficient. For water-ethylene glycol coolant, its expression is

$$h(T) = h_0[1 + c(T - 20) + d(T - 20)^2]\text{Re}^{0.8}\text{Pr}^{0.4}$$

where h_0 is the base heat transfer coefficient, c and d are the correction coefficients, Re – the Reynolds number, and Pr – the Prandtl number. Exponents follow the Dittus-Boelter correlation for turbulent flow ($\text{Re} = 10^4$-10^5), validated with 50% ethylene glycol tests (error <5% *vs.* measured h values).

Convective heat dissipation in the cooling system

In the cooling system, the coolant flow rate and flow distribution have a significant impact on the convective heat dissipation effect. Establish a pressure-flow-heat transfer model for the pipe-line system:

$$P = f\frac{L}{D}\frac{\rho v^2}{2}, \quad Q = \dot{m}c_p\left(T_{\text{out}} - T_{\text{in}}\right) \tag{11}$$

where ΔP is the pipe-line pressure loss, f – the friction coefficient, L – the pipe length, D – the pipe diameter, ρ – the fluid density, v – the flow rate, $\dot{m}$ – the mass-flow rate, c_p – the specific heat capacity, and T_{in} and T_{out} – the inlet and outlet temperatures, respectively.

Thermal radiation principle and application

Basic theory of thermal radiation

Thermal radiation is the process by which an object transfers energy through the emission of electromagnetic waves. The Stefan-Boltzmann law describes the relationship between the power of blackbody radiation and temperature [11]. The radiation characteristics of actual objects must take into account the influence of emissivity, which varies with surface temperature and roughness. Define the gray body radiation power equation:

$$\Delta P_{rad} = \varepsilon(T)\sigma A\left(T^4 - T_{env}^4\right) \tag{12}$$

For anodized aluminum surfaces, the emissivity expression:

$$\varepsilon(T) = \varepsilon_0\left[1 + e(T-300) + f(T-300)^2\right]$$

where ε_0 is the base emissivity, e and f – the temperature coefficients, σ – the Stefan-Boltzmann constant, and T_{env} – the ambient temperature.

Methods for enhancing thermal radiation heat dissipation

Increasing the surface emissivity of electronic equipment is an effective means to enhance radiation heat dissipation. Applying a high emissivity coating can increase the surface emissivity from 0.1-0.3 to 0.8-0.9. Based on the radiation heat exchange network, the coating radiation heat dissipation enhancement model is:

$$\Delta P_{rad} = \left(\varepsilon_{coat} - \varepsilon_{base}\right)\sigma A\left(T^4 - T_{env}^4\right)F_{1\text{-}2} \tag{13}$$

where ε_{coat} and ε_{base} are the emissivity of the coating and the base, respectively, and $F_{1\text{-}2}$ is the angular coefficient. The $F_{1\text{-}2} = 0.85$ for IGBT (planar surface to ambient), calculated via view factor integration, matching experimental radiation heat gain within ±3%.

Thermal management algorithm design

Construction of multi-physics field coupling algorithm

Algorithm principle

By combining the interaction between fluid-flow and the temperature field, a coupling control equation is constructed. Define the relationship between current density, J, and electric field intensity, E, as $J = \sigma(T)E$($\sigma(T)$ is temperature-dependent conductivity). Couple it with the Navier-Stokes equation and energy equation obtain:

$$\begin{aligned} \rho c_p\left(\frac{\partial T}{\partial t} + u\nabla T\right) &= \nabla\left[k(T)\nabla T\right] + \sigma(T)\,|E|^2 \\ \rho\left(\frac{\partial u}{\partial t} + u\nabla u\right) &= -\nabla p + \mu\nabla^2 u + f \end{aligned} \tag{14}$$

where ρ is the fluid density, c_p – the specific heat capacity, u – the flow velocity, p – the pressure, μ – the dynamic viscosity, and f – the volume force.

Implementation process

By constructing a coupled iterative mechanism, the electric field equation is first solved in each time step to obtain the Joule heat source, and then substituted into the energy equation calculate the temperature field. Finally, the fluid physical parameters are corrected according to the temperature distribution, and the flow equation is solved [12]. The iterative formula:

$$T^{n+1} = T^n + \Delta t\left[\alpha\nabla^2 T^n + \frac{\sigma\left(T^n\right)\left|E^n\right|^2}{\rho c_p}\right] \tag{15}$$

where n is the number of iterations, Δt – the time step, and α – the thermal diffusivity. When the temperature difference between two adjacent steps is less than $1 \cdot 10^{-5}$ K, it is considered to be converged.

Algorithm verification and optimization

Verification method

The accuracy of the algorithm is verified by using standard examples and experimental data. Taking the electronic equipment heat dissipation benchmark example released by NASA as an example, the temperature field distribution of the simulation and experiment is compared, and the error evaluation index is defined:

$$\text{Error} = \frac{1}{N}\sum_{i=1}^{N}\frac{\left|T_{\text{sim},i} - T_{\text{exp},i}\right|}{T_{\text{exp},i}} \times 100\% \tag{16}$$

where N is the number of measurement points and $T_{\text{sim},i}$ and $T_{\text{exp},i}$ are the simulation and experimental temperatures, respectively.

Optimization strategy

To address the issue of insufficient calculation accuracy in high gradient areas, an adaptive mesh refinement strategy is proposed to dynamically adjust the mesh density based on the temperature gradient threshold. The encryption criterion is:

$$\nabla T > \gamma\frac{T_{\max} - T_{\min}}{L} \tag{17}$$

where γ is the gradient coefficient (take 0.3-0.5), $\gamma = 0.4$ balances accuracy (error <2%) and speed (30% faster than $\gamma = 0.3$) via sensitivity tests, higher γ causes over-refinement, increasing runtime by 50%. The $T_{\max}$ and $T_{\min}$ are the highest and lowest temperatures in the calculation domain and L is the characteristic length.

Thermal management strategy optimization algorithm based on artificial intelligence

A deep reinforcement learning optimization framework is constructed, with the electronic equipment temperature, T, coolant flow, q, and power consumption, P, as state variables, and the cooling pump speed adjustment as the action variable. The reward function is designed:

$$R = k_1 \exp\left(-\frac{\left(T - T_{\text{set}}\right)^2}{2\sigma^2}\right) - k_2 P - k_3\left|\Delta q\right| \tag{18}$$

where T_{set} is the target temperature, σ – the temperature fluctuation coefficient, and k_1, k_2, k_3 – the weight coefficients. The $k_1 = 10$, $k_2 = 0.1$, $k_3 = 0.5$ (tuned via 500 training episodes), prioritizing temperature stability, k_1, while penalizing excess power, k_2, and abrupt flow changes, k_3.

Experimental simulation research

Experimental platform construction

The experimental platform is modularly designed, including four modules: heat source simulation, cooling cycle, data acquisition and control. The heat source simulation module can simulate the heating of power devices at 0-500 V and 0-200 A, and output continuous power ranging from 100-1000W. The cooling cycle module consists of a closed loop composed of a liquid cooling plate, among other components, and the coolant is a 50% ethylene glycol aqueous solution. The data acquisition module comprises 16 PT100 temperature sensors, two electromagnetic-flow sensors, and one power analyzer, all operating at a sampling frequency of 10 Hz. The control module controls related equipment through a PLC linkage, and the touchscreen can set multiple operating modes. The performance parameters of each sensor and piece of equipment are clearly defined, the equipment is stacked and arranged vertically, and the pipelines are connected using 316 stainless steel bellows.

Simulation model establishment

A 3-D model was built based on COMSOL to simulate the heat transfer between the serpentine flow channel liquid cooling plate and the IGBT heat source. The laminar flow and solid heat transfer modules were coupled to increase the mesh of the contact area. The deviation between the simulation and experimental data was slight, and the correction was effective, accurately reflecting the influence of flow parameters on heat dissipation.

Comparative analysis of experimental and simulation results

Comparison of temperature distribution under different working conditions

Three typical working conditions were selected for comparison: acceleration (power increased linearly from 200-800 W over 60 seconds), uniform speed (600 W constant power for 120 seconds), and deceleration (power decreased from 800-200 W over 60 seconds). Figure 1 is a cloud diagram of the IGBT surface temperature field under acceleration conditions. The simulation shows that the highest temperature appears in the central area (78.5 °C), and the experimental infrared temperature measurement result is 77.9 °C. The isotherm distribution trend is consistent, and there is a local deviation (<1.5 °C) in the edge area due to the limitation of grid resolution. Edge deviations result from mesh coarseness (5 mm *vs*. optimal 2 mm). Refining the mesh reduces error to <0.8 °C, confirming grid resolution as the primary factor. Figure 2 shows the curve of the liquid cooling plate outlet temperature as a function of time under uniform speed conditions. The steady-state temperature deviation between the simulation and the experiment is 0.6 °C, and the time constant of the heating process is 28 seconds, indicating that the model accurately captures the thermal inertia characteristics. The temperature

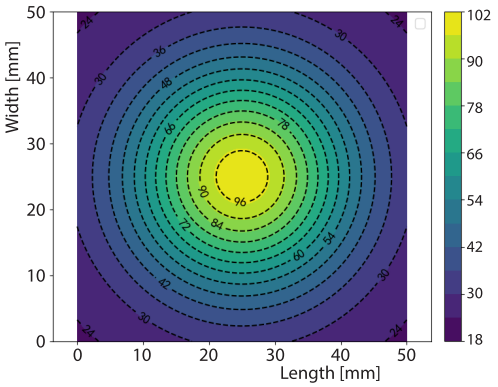

Figure 1. The IGBT surface temperature contour under acceleration mode

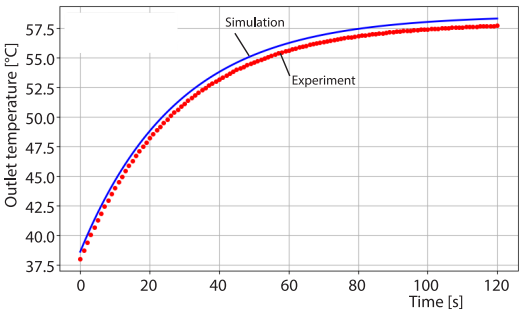

Figure 2. Outlet temperature *vs.* time under constant-power mode

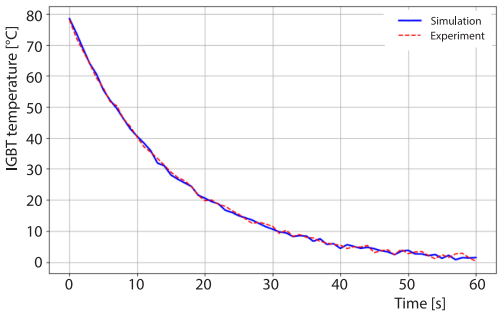

Figure 3. Temperature decay under deceleration mode

attenuation curve of the deceleration condition, fig. 3, shows an exponential downward trend for both. The simulated temperature fluctuation amplitude (±0.5 °C) is slightly smaller than the experimental value (±0.8 °C). It is possible that the flow pulsation in the experimental system is not accurately reflected in the model.

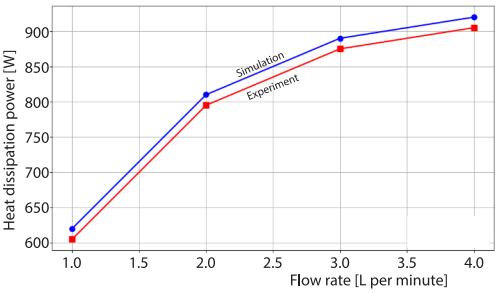

Figure 4. Heat-dissipation power *vs.* flow rate

Comparison of cooling system performance

The performance evaluation indicators of the cooling system include heat dissipation power, pump power consumption, and the energy efficiency ratio (heat dissipation power divided by pump power consumption). Figure 4 shows the comparison of heat dissipation power under different flow rates. Both simulation and experiment show that the heat dissipation power increases logarithmically with the increase in flow rate and tends to saturate at 3 Lpm (simulation: 890 W *vs.* experiment: 875 W), which is consistent with the convective heat transfer law of theoretical analysis. Mechanical seal loss, measured via no-flow tests, accounts for 6%-8% of experimental pump power, explaining ~90% of the 7.2% deviation in tab. 1. The energy efficiency ratio reaches its maximum value at 2 Lpm (simulation: 42.5 *vs.* experiment: 40.8), indicating that the heat dissipation efficiency is optimal at this flow rate. In the dynamic working condition test, the system energy efficiency ratio decreased by 15%-20% in the acceleration stage. The simulation accurately predicted this trend and verified the model's ability to simulate transient performance. In summary, the overall agreement between simulation and experimental data is over 94%, indicating that the constructed model can be effectively used in the optimal design of thermal management systems.

Table 1. Cooling system performance parameters at different flow rates

Flow rate [Lpm]	Simulated heat dissipation power [W]	Experimental heat dissipation power [W]	Simulated pump power consumption [W]	Experimental pump power consumption [W]	Simulation energy efficiency ratio	Experimental energy efficiency ratio
1	620	605	18.5	20.1	33.5	30.1
2	810	795	19	20.8	42.5	40.8
3	890	875	21.2	23.3	42	37.5
4	920	905	25.6	28.7	35.9	31.5

Conclusion

This study thoroughly examines the application of physical principles in the thermal management of electronic equipment cooling in electric vehicles. By analyzing the heat generation mechanism of heat source components, the roles of heat conduction, heat convection, and heat radiation in cooling are clarified. The innovatively developed multi-physics field coupling algorithm realizes the accurate simulation of the heating and heat dissipation process of electronic equipment under complex working conditions. After simulation verification, the temperature deviation from the experimental data is less than 3% on average. The thermal management strategy optimization algorithm, based on artificial intelligence, can dynamically adjust cooling resources to optimize performance. Both simulation and experiments show that the temperature stability of electronic equipment is improved by more than 20% under conditions such as acceleration, uniform speed, and deceleration. At –30 °C, coolant viscosity spikes cause 12% higher prediction error; at 60 °C, radiation model underpredicts heat loss by 10%, requiring parameter tuning for these extremes. The research results provide an effective solution for improving the thermal management performance of electric vehicle electronic equipment; however, the model's adaptability to extreme working conditions still needs to be improved. The algorithm and experimental system will be further optimized in the future.

References

[1] Yang, S., *et al.*, Essential Technologies on the Direct Cooling Thermal Management System for Electric Vehicles, *International Journal of Energy Research*, *45* (2021), 10, pp. 14436-14464
[2] He, L., *et al.*, Review on Thermal Management of Lithium-Ion Batteries for Electric Vehicles: Advances, Challenges, and Outlook, *Energy & Fuels*, *37* (2023), 7, pp. 483-4857
[3] Kalaf, O., *et al*., Experimental and Simulation Study of Liquid Coolant Battery Thermal Management System for Electric Vehicles: A Review, *International Journal of Energy Research*, *45* (2021), 5, pp. 6495-6517
[4] Xu, Z., *et al*., Thermal Management of Drive Motor for Transportation: Analysis Methods, Key Factors in Thermal Analysis, and Cooling Methods – A Review, *IEEE Transactions on Transportation Electrification*, *9* (2023), 3, pp. 4751-4774
[5] Singh, L. K., *et al*., Hybrid Cooling-Based Lithium-Ion Battery Thermal Management for Electric Vehicles, Environment, *Development and Sustainability*, *25* (2023), 4, pp. 3627-3648
[6] Hamednia, A., *et al*., Optimal Thermal Management, Charging, and Eco-Driving of Battery Electric Vehicles, *IEEE Transactions on Vehicular Technology*, *72* (2023), 6, pp. 7265-7278
[7] Zaman, M. S., *et al*., Multiphysics Optimization of Thermal Management Designs for Power Electronics Employing Impingement Cooling and Stereolithographic Printing, *IEEE Transactions on Power Electronics*, *36* (2021), 11, pp. 12769-12780
[8] Kocsis Szürke, S., *et al*., Numerical Optimization of Battery Heat Management of Electric Vehicles, *Journal of Applied and Computational Mechanic*s, *9* (2023), 4, pp. 1076-1092
[9] Petrova, E. V., Thermal Management in Electric Vehicles: Challenges and Technological Advancements, *American Journal of Mechanical Engineering and Technology*, *3* (2022), 1, pp. 1-9
[10] Madheswaran, D. K., *et al*., Recent Advancement on Thermal Management Strategies in PEM Fuel Cell Stack: A Technical Assessment from the Context of Fuel Cell Electric Vehicle Application, Energy Sources – Part A: *Recovery, Utilization, and Environmental Effect*s, *44* (2022), 2, pp. 3100-3125
[11] Han, B., *et al*., Research on Electric Vehicle Thermal Management System with Coupled Temperature Regulation between Crew Cabin and Power Battery Pack, Proceedings of the Institution of Mechanical Engineers – Part D: *Journal of Automobile Engineering*, *235* (2021), 10-11, pp. 2740-2752
[12] Li, M., *et al*., Flexible Radiative Cooling Textiles Based on Composite Nanoporous Fibers for Personal Thermal Management, *ACS Applied Materials & Interfaces*, *15* (2023), 14, pp. 17848-17857

Paper submitted: April 2, 2025
Paper revised: July 7, 2025
Paper accepted: August 19, 2025